JACS
JOURNAL OF THE AMERICAN CHEMICAL SOCIETY
Article
pubs.acs.org/JACS

Minimal Proton Channel Enables H_2 Oxidation and Production with a Water-Soluble Nickel-Based Catalyst

Arnab Dutta, Sheri Lense, Jianbo Hou, Mark H. Engelhard, John A. S. Roberts,* and Wendy J. Shaw*

Pacific Northwest National Laboratory, Richland, Washington 99352, United States

Supporting Information

ABSTRACT: Hydrogenase enzymes use first-row transition metals to interconvert H_2 with protons and electrons, reactions that are important for the storage and recovery of energy from intermittent sources such as solar, hydroelectric, and wind. Here we present $Ni(P^{Cy}_2N^{Gly}_2)_2$, a water-soluble molecular electrocatalyst with the amino acid glycine built into the diphosphine ligand framework. Proton transfer between the outer coordination sphere carboxylates and the second coordination sphere pendant amines is rapid, as observed by cyclic voltammetry and FTIR spectroscopy, indicating that the carboxylate groups may participate in proton transfer during catalysis. This complex oxidizes H_2 (1−33 s^{-1}) at low overpotentials (150−365 mV) over a range of pH values (0.1−9.0) and produces H_2 under identical solution conditions (>2400 s^{-1} at pH 0.5). Enzymes employ proton channels for the controlled movement of protons over long distances—the results presented here demonstrate the effects of a simple two-component proton channel in a synthetic molecular electrocatalyst.

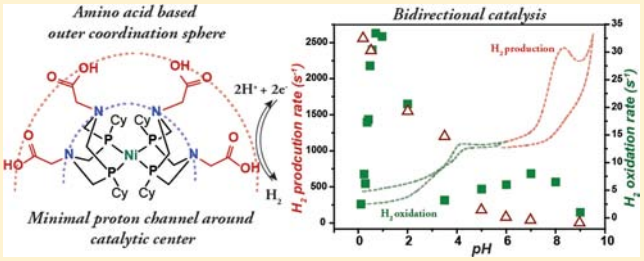

INTRODUCTION

Hydrogenases are nature's enzymes used in the microbial world to interconvert protons and H_2 (eq 1) to control energy

$$2H^+ + 2e^- \rightleftharpoons H_2 \quad (1)$$

processes. The rates are fast, as high as 20,000 s^{-1} depending on the specific enzyme and reaction direction.[1] These enzyme-catalyzed reactions are also typically reversible,[2] indicating that the enzymes can interconvert H_2 and protons at low overpotentials, i.e., with little excess driving force, the desired condition for the most energy efficient catalytic process.[3] Rapid catalysis at low overpotentials is achieved in enzymes by coupling the active site with the enzyme's protein scaffold or outer coordination sphere, which provides precise control over the catalytic process.[4] One important feature of outer coordination sphere control is the use of proton channels to achieve precise and fast proton delivery to and from the active site.[1a] Notably, synthetic molecular electrocatalysts for H_2 production and oxidation deliver and remove protons less effectively than the hydrogenase enzymes and require larger applied potentials to mediate catalysis.[3,5] These complexes are often functional only in organic solvents, a barrier to their direct application in fuel cells.

Using functional rather than structural mimicry of enzymes as a design principle,[3] impressive enhancements in rate have been achieved by incorporating pendant amine proton relays into the second coordination sphere of the $Ni(P^R_2N^{R'}_2)_2$ catalysts (where P_2N_2 = 1,5-diaza-3,7-diphosphacyclooctane, Figure 1), mimicking the function of the proton relay in the active site of [FeFe]-hydrogenase.[6] Building upon this functional approach, faster and more efficient catalysis may be realized by introducing additional enzyme-like functionality such as amino acids or peptides into the outer coordination sphere of molecular catalysts. Rate enhancements have already been achieved by incorporating amino acids in the outer coordination sphere of $Ni(P^{Ph}_2N^{R'}_2)_2$ H_2 production catalysts, demonstrating the validity of this extension to the design of functional mimics.[7] In this work, we extend this approach by building a $Ni(P^{Cy}_2N^{R'}_2)_2$ complex with a second set of proton relays that interact directly with the pendant amines. We introduce an amino acid into the outer coordination sphere to produce a simple two-relay proton channel that enhances proton movement to and from the metal center. The resulting complex is water-soluble and is active for H_2 oxidation while operating with a low overpotential.

RESULTS AND DISCUSSION

Characterization under N_2. Glycine was incorporated directly into the P_2N_2 ligand and metalated to make $[Ni^{II}(P^{Cy}_2N^{Gly}_2)_2]^{2+}$, and its derivative, $[Ni^0(P^{Cy}_2N^{Gly*}_2)_2]^-$ (Figure 1), which by design have moderate thermodynamic biases toward H_2 oxidation.[5b] The $P^{Cy}_2N^{Gly}_2$ ligand and $[Ni^{II}(P^{Cy}_2N^{Gly}_2)_2]^{2+}$ metal complex were synthesized in a manner similar to other complexes of this type.[8] Mass spectrometry, ^1H NMR, ^{13}C NMR and ^{31}P NMR are all consistent with the structures shown for both the ligand and the metal complexes. After several hours under N_2, the

Received: July 29, 2013
Published: November 8, 2013

   dx.doi.org/10.1021/ja407826d | J. Am. Chem. Soc. 2013, 135, 18490−18496

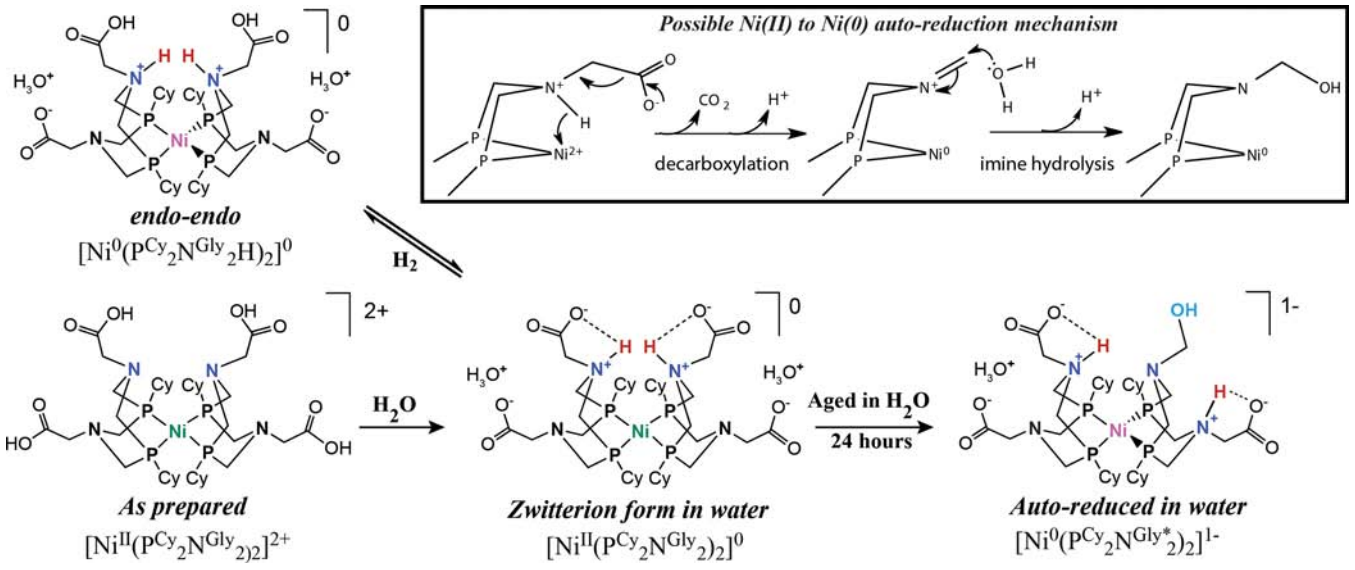

Figure 1. Structure of $[Ni^{II}(P^{Cy}_2N^{Gly}_2)_2]^{2+}$ as prepared (bottom left), upon dissolution in water to form the zwitterionic complex (bottom center), after H_2 addition (top left), and upon aging in water (bottom right). Inset: Proposed autoreduction mechanism for the formation of $[Ni^0(P^{Cy}_2N^{Gly*}_2)_2]^-$ species.

unbuffered aqueous solution of $[Ni^{II}(P^{Cy}_2N^{Gly}_2)_2]^{2+}$ loses its characteristic red color to become pale yellow, which is more consistent with Ni(0) complexes (Figure S1).[8b] The ^{31}P NMR spectrum also changes, becoming indistinguishable from that of the Ni(0) H_2 addition product $[Ni^0(P^{Cy}_2N^{Gly}_2H)_2]^0$ (Figure S2), indicating protonation of the pendant amines and a two-electron reduction at the metal center. X-ray photoelectron spectroscopy (XPS) confirms the conversion to Ni(0) (Figure S3). Further investigation by gas chromatography, mass spectrometry, and ^{13}C NMR revealed the evolution of 1 equiv of CO_2 per Ni, affording a -NCH_2OH group (Figure 1 and Figure S4). This conversion has been noted in other systems and is suggested to proceed via an imine intermediate (Figure 1, inset).[9] This new complex, which still has three carboxylates intact, is referred to herein as $[Ni^0(P^{Cy}_2N^{Gly*}_2)_2]^-$. Decarboxylation does not appear to influence either the stoichiometric or catalytic voltammetry; however, to ensure reproducibility, we have used $[Ni^0(P^{Cy}_2N^{Gly*}_2)_2]^-$ for all catalytic studies.

Cyclic voltammetry of $[Ni^{II}(P^{Cy}_2N^{Gly}_2)_2]^{2+}$ in methanol under N_2 (Figure 2) exhibits one broad feature with $E_{1/2}$ = −0.76 V vs ferrocenium/ferrocene ($FeCP_2^{+/0}$, the reference potential used throughout) with a peak-to-peak separation ΔE_p = 142 mV consistent with two overlapping one-electron waves. The data in water is substantially similar, though the waves are less well resolved and the features are complicated by the catalytic processes discussed below (Figure S9). Measured peak currents in both water and methanol are larger than predicted for a one-electron reduction (determined using the Randles−Sevcik equation[10] with the catalyst diffusion coefficient measured as described in the Materials and Methods) and no additional reduction waves are seen upon scanning to −1.5 V, consistent with this interpretation. A similar feature is observed in acetonitrile. By comparison, the related complex, $[Ni(P^{Cy}_2N^{Bn}_2)_2]^{2+}$, in acetonitrile shows two well-separated waves typical of $Ni(P^R_2N^{R'}_2)_2$ complexes and corresponding to the Ni(II/I) and Ni(I/0) redox couples ($E_{1/2}$ = −0.78 V, ΔE_p = 82 mV and −1.33 V, ΔE_p = 68 mV, stripping of adsorbed material is observed upon reoxidation of Ni(0); Figure S5).[8]

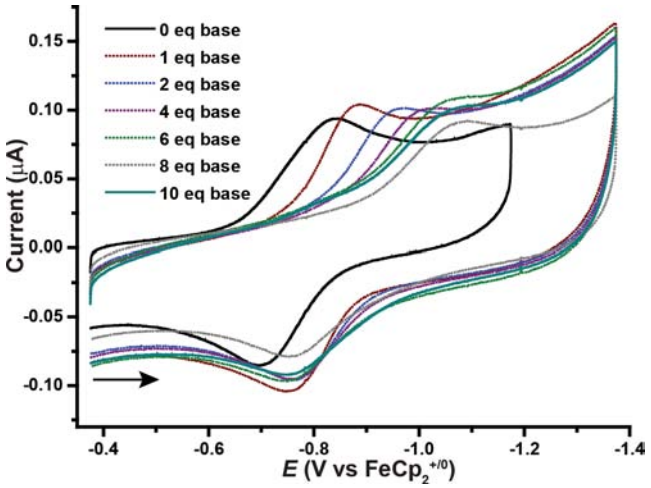

Figure 2. Cyclic voltammetry of $[Ni^{II}(P^{Cy}_2N^{Gly}_2)_2]^{2+}$ (0.05 mM) in neutral methanol (0.05 M $^nBu_4N^+$TFAB) (TFAB = tetrakisfluoroarylborate) and with 1, 2, 4, 6, 8, and 10 equiv added triethylamine, collected with ν = 0.1 V s^{-1}.

Given the structural and electronic similarity of $[Ni^{II}(P^{Cy}_2N^{Gly}_2)_2]^{2+}$ and $[Ni^{II}(P^{Cy}_2N^{Bn}_2)_2]^{2+}$, the differences observed in the voltammetry must be due to the carboxylic acid/carboxylate groups themselves. Adding 1−8 equiv of triethylamine shifts this single reduction feature to more negative values (Figure 2; data in aqueous solution are shown in Figure S9). This dependence on added base indicates that the reduction potential is influenced by the protonation state of the Ni(II) species. There is essentially no dependence on the scan rate (0.05−5 V s^{-1}; Figure S8), indicating that the intervening chemical steps are rapid on the experimental time scale.

The dependence of the voltammetry on the protonation state suggests two interpretations: (i) rapid intramolecular proton movement, and (ii) reversible COO^- binding to Ni(II) upon

dx.doi.org/10.1021/ja407826d | J. Am. Chem. Soc. 2013, 135, 18490−18496

deprotonation of COOH. These processes may influence the voltammetry differently for different protonation states. Without added base, the $[Ni^{II}(P^{Cy}_2N^{Gly}_2)_2]^{2+}$ is reduced by two electrons at a potential slightly positive of the Ni(II/I) potential of $[Ni(P^{Cy}_2N^{Bn}_2)_2]^{2+}$. Since the II/I and I/0 couples are overlapping for $[Ni^{II}(P^{Cy}_2N^{Gly}_2)_2]^{2+}$, this indicates that the Ni(I/0) couple has shifted positive. This observation is consistent with fast proton movement: if reduction to Ni(I) triggers proton transfer from COOH to N (or from N to Ni), this would facilitate the second reduction step, shifting the Ni(I/0) potential to more positive values (this is detailed in the SI and Figure S7).[11] The voltammetry observed prior to adding base cannot be the result of COO^- binding to Ni(II), since this interaction would not influence the Ni(I/0) couple and would shift the Ni(II/I) couple to more *negative* values, as observed by Seu and co-workers in studies with a related $[Ni(P^R_2N^{R'}_2)_2]^{2+}$ complex upon adding acetate.[12] Interaction between COO^- and Ni(I) is unlikely since Ni is tetrahedral in this state and coordinatively saturated.[12]

Although the voltammetry of the fully protonated $[Ni^{II}(P^{Cy}_2N^{Gly}_2)_2]^{2+}$ complex may be explained by proton movement alone, if proton movement were the only process occurring, one would expect to see separate Ni(II/I) and Ni(I/0) waves upon complete deprotonation. However, the fully deprotonated species is still reduced in two overlapping one electron waves, in this case at potentials near the Ni(I/0) couple of the parent $[Ni(P^{Cy}_2N^{Bn}_2)_2]^+$ complex (−1.33 V vs $FeCP_2^{+/0}$). Since this cannot be due to proton movement, another explanation, possibly COO^- binding to Ni(II), is necessary. Parallel ^{31}P NMR and FTIR studies indicate that this interaction, if it occurs, is labile.[13] While the data suggest that COO^- binding may be relevant, the more important conclusion in the context of catalysis is that fast proton transfer between the COOH groups and the pendant amines is triggered by changing the oxidation state of Ni.

The FTIR spectrum of $[Ni^{II}(P^{Cy}_2N^{Gly}_2)_2]^{2+}$ in methanol under N_2 (Figure 3) provides further evidence of facile proton movement. Spectroscopic features consistent with both ammonium (NH bending mode; ν = 1640 cm^{-1})[14] and carboxylate groups (ν = 1605 and 1575 cm^{-1}, confirmed by comparison with the FTIR spectrum of the free ligand following deprotonation, Figure S10) indicate intramolecular proton transfer from the COOH groups to the more basic pendant amines, creating the zwitterionic form (Figure 1). This is expected to occur for only one glycine group on each ligand, since protonation of both amines on a single ligand is predicted to be disfavored by ∼6 kcal/mol.[15] The FTIR spectrum also has a COOH stretching frequency at 1730 cm^{-1}. The non-zwitterionic glycines are expected to remain protonated based on a pK_a of 4.0 for the COOH groups of $[Ni^{II}(P^{Cy}_2N^{Gly}_2)_2]^{2+}$ in methanol (Figure S11) vs. the solution pH of 3.4. It should be noted that in water, the pK_a value for the COOH groups in $[Ni^{II}(P^{Cy}_2N^{Gly}_2)_2]^{2+}$ is 2.5 (Figure S12), indicating that the deprotonated form of the two non-zwitterionic glycines should predominate in neutral aqueous solution (Figure 1).[16] The FTIR and electrochemistry data are both consistent with the exchange of protons between the glycine pendant amines and carboxylate groups, thereby creating a proton channel.

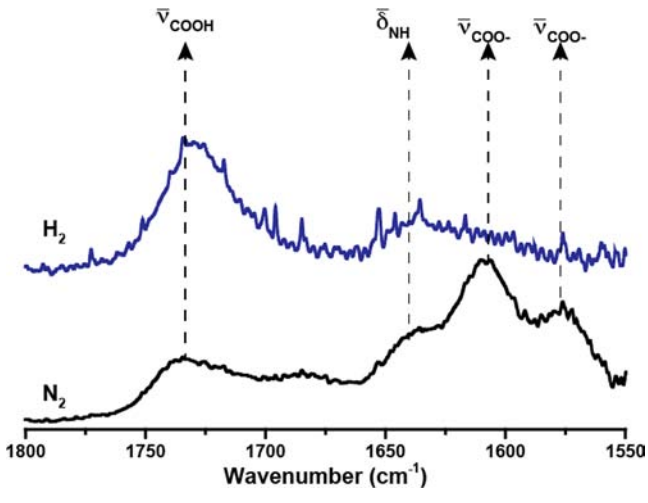

Figure 3. FTIR data in methanol, showing that the −COOH groups of the $[Ni^{II}(P^{Cy}_2N^{Gly}_2)_2]^{2+}$ species under N_2 (black solid line) are partially deprotonated, creating the zwitterionic form. Addition of H_2 fully protonates the complex, resulting in four −COOH groups, demonstrating facile proton movement between the carboxylate groups and the pendant amines.

Characterization under H_2 with Added Base. Upon addition of H_2, the complex converts from the zwitterionic Ni(II) species ($[Ni^{II}(P^{Cy}_2N^{Gly}_2)_2]^{2+}$) to the doubly N-protonated Ni(0) tetracarboxylic acid ($[Ni^0(P^{Cy}_2N^{Gly}_2H)_2]^{2+}$), changing in color from red to pale yellow. Based on the $^{31}P\{^1H\}$ NMR spectrum in water (Figure S2), the addition of H_2 to the metal complex results in a single isomer with protons oriented toward the Ni center (endo-endo, Figure 1).[5b,17] The FTIR spectrum of the H_2 addition complex in methanol is consistent with fully protonated COOH groups (Figure 3). This suggests that when H_2 adds, protons on the pendant amines are displaced to the COO^- groups, providing strong evidence that the zwitterionic form shown in Figure 1 is present prior to H_2 addition. This is confirmed by the disappearance of the COOH IR bands (Figure S13) observed upon adding 6 equiv of base to $[Ni^0(P^{Cy}_2N^{Gly}_2H)_2]^{2+}$ in methanol.

Catalysis. The $[Ni^0(P^{Cy}_2N^{Gly*}_2)_2]^-$ complex is active for electrocatalytic H_2 oxidation, with a TOF of 8 s^{-1} at pH = 7.0, operating at an overpotential of 285 mV determined at the half-height of the catalytic wave ($E_{cat/2}$). Catalysis under these conditions is homogeneous on the basis of the rinse test method (Figure S14).[19] Rates were determined using eq 2,[20] where D is the diffusion coefficient of the catalyst (3.0×10^{-6} cm^2/s), A is the surface area of the electrode (9.23×10^{-3} cm^2, Figure S15), n is the number of electrons for the catalytic process (2), F is Faraday's constant. and i_{cat} is the catalytic current.

$$k_{obs} = \frac{1}{D}\left(\frac{i_{cat}}{nFA[cat]}\right)^2 \quad (2)$$

Hydrogen oxidation was investigated over a range of pH values, from 0.1 to 9.0 (Table 1, Figure 4, Figure 5). The TOF as a function of pH has two maxima, one at pH 7.0 (TOF = 8 s^{-1}) and another at pH 0.7 (33 s^{-1}). Interestingly, the overpotential decreases as the rates increase (Table 1), with an overpotential of 150−160 mV at the highest rates (equilibrium potentials and $E_{cat/2}$ values are given in Table S2). The relatively large increase in rate up to pH 0.7 correlates with the increase in the degree of protonation of the carboxylate groups. This observation is thought to be due to the disruption of the stable interaction (salt bridge) between the R_3NH^+ and the COO^-. The rapid drop in catalytic activity below 0.7 is likely

dx.doi.org/10.1021/ja407826d | J. Am. Chem. Soc. 2013, 135, 18490−18496

Table 1. TOFs and Overpotentials for H_2 Oxidation with $[Ni^0(P^{Cy}_2N^{Gly*}_2)_2]^-$ in Water at Different pH Values

pH	TOF (s^{-1})	overpotential (mV)
0.1	3	180
0.2	8	170
0.3	6	170
0.4	17	155
0.5	28	160
0.6	30	155
0.7	33	150
1.0	33	160
2	21	160
3.5	3	240
5	5	265
6	6	270
7	8	285
8	7	325
9	1	365

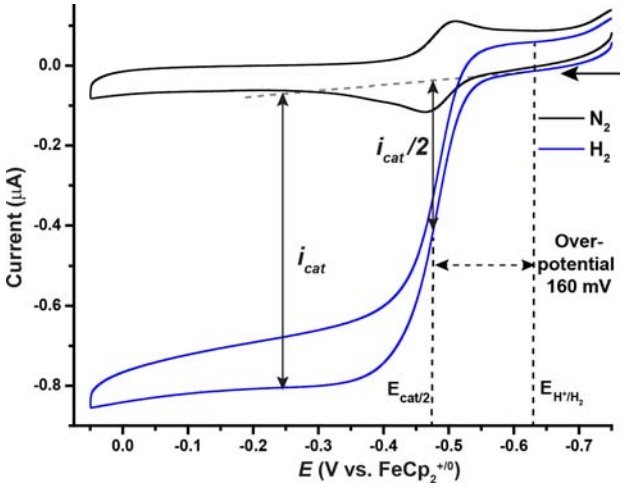

Figure 4. Cyclic voltammogram of $[Ni^0(P^{Cy}_2N^{Gly*}_2)_2]^-$ (0.050 mM) under N_2 in water at pH 2.0 (black) and under H_2 (blue). Addition of H_2 results in a catalytic current enhancement consistent with H_2 oxidation, with a turnover frequency of 21 s^{-1} and an overpotential of 160 mV. Conditions: 0.01 M $HClO_4$, 0.1 M $NaClO_4$ aqueous solution, 1 mm glassy carbon disk working electrode, Ag/AgCl in saturated KCl reference electrode, scan rate 50 mV/s.

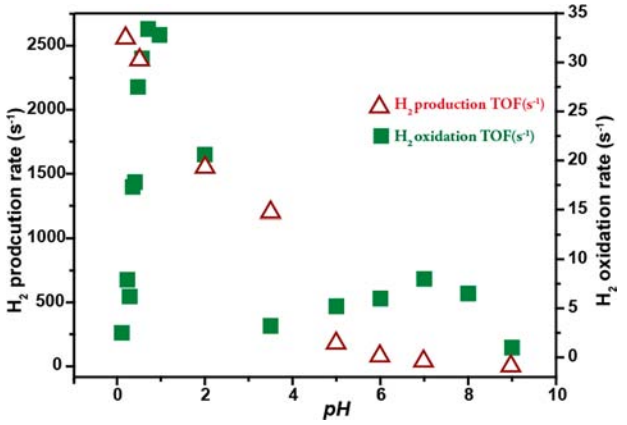

Figure 5. Catalysis of $[Ni^0(P^{Cy}_2N^{Gly*}_2)_2]^-$ as a function of pH in water: H_2 oxidation rates (green squares, under 1 atm. H_2) and H_2 production (brown triangles, under N_2). Conditions: either 0.1 M MES/HEPES (buffered pH 3.5–9 solutions) or adjusted with $HClO_4$ (unbuffered pH 0.1–2 solutions) in 0.1 M $NaClO_4$ aqueous solution, 1 mm glassy carbon disk working electrode, Ag/AgCl in saturated KCl reference electrode, scan rate 1 V/s for H_2 production, 50 mV/s for H_2 oxidation.

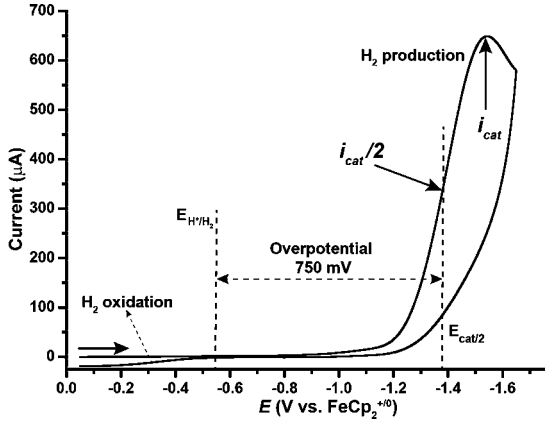

Figure 6. Cyclic voltammogram of $[Ni^0(P^{Cy}_2N^{Gly*}_2)_2]^-$ (0.080 mM) under N_2 in acidic water (pH 0.5) demonstrates proton reduction at −1.5 V with a turnover frequency of >2400 s^{-1} and an overpotential of 750 mV. Conditions: 0.3 M $HClO_4$, 0.1 M $NaClO_4$ aqueous solution, pH 0.5, 1 mm glassy carbon disk working electrode, Ag/AgCl in saturated KCl reference electrode, scan rate 1 V/s.

due to protonation of the third and/or fourth pendant amines, limiting the ability to add H_2. We are currently investigating the mechanistic details of this observation using experimental methods and computational analysis.

These rates are among some of the fastest H_2 oxidation catalysts reported to date (up to 58 s^{-1} in MeCN)[5b,21] and the overpotential at $E_{cat/2}$ is lower as well (150 mV vs the reported value for the fastest catalyst of ∼500 mV using triethyl amine as a base).[21] The rate of H_2 oxidation with $[Ni^0(P^{Cy}_2N^{Gly*}_2)_2]^-$ in methanol is four times faster,[22] and the solubility of H_2 in methanol is ∼3.5 times higher than in water,[23] suggesting that H_2 addition is rate-limiting in both solvents, consistent with rapid proton movement. This observation is currently under investigatation.

The $[Ni^0(P^{Cy}_2N^{Gly*}_2)_2]^-$ complex can also catalyze H_2 production (Figure 6). The current enhancement at −1.5 V was demonstrated to be due to H_2 evolution on the basis of electrochemistry performed under N_2 (Figure S16). H_2 production can be observed at all of the pH values studied (0.1–9), with more acidic conditions favoring faster catalysis (Figure 5). Further electrochemical experiments confirmed that H_2 production was the result of the $[Ni^0(P^{Cy}_2N^{Gly*}_2)_2]^-$ complex adhering to the electrode surface (Figures S17 and S18), introducing uncertainty in the rate determination due to the unknown coverage of active catalyst on the surface. A lower limit of 2400 s^{-1} in acidic solution (pH 0.5) was estimated assuming a close-packed monolayer of adsorbed, active catalyst (see SI). Under these conditions the overpotential at $E_{cat/2}$ is 750 mV; at pH 6.0, the rate is >80 s^{-1} and the overpotential at $E_{cat/2}$ is 250 mV.

While the optimal conditions for H_2 oxidation and production are different, both are observed in the same solution at all pH values. Once the catalytic plateau for H_2 oxidation is reached, reversing the scanning direction to more

dx.doi.org/10.1021/ja407826d | J. Am. Chem. Soc. 2013, 135, 18490–18496

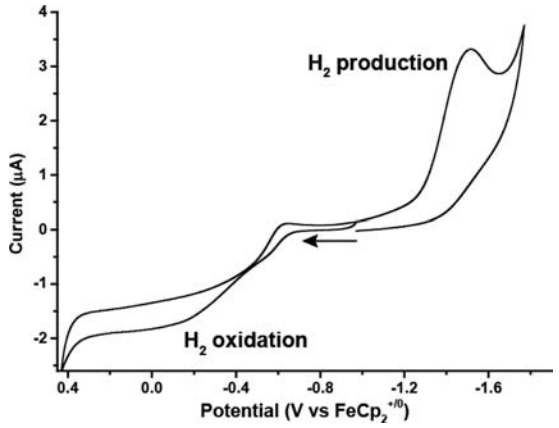

Figure 7. $[Ni^0(P^{Cy}_2N^{Gly*}_2)_2]^-$ operates bidirectionally in water without externally added acid or base. Data at pH 5.0 are shown, where H_2 oxidation is operating at 5 s^{-1} and H_2 production has a lower limit of ~100 s^{-1}. Conditions: 0.1 M MES/HEPES, 0.1 M $NaClO_4$ aqueous solution, 1 mm glassy carbon disk working electrode, Ag/AgCl in saturated KCl reference electrode, scan rate 50 mV/s.

negative potentials results in an increase in cathodic current at −1.5 V, consistent with H_2 production catalysis (Figure 7; no change in solution composition was needed to observe this current enhancement). Catalysis was observed upon repeated cycling through the H_2 production and oxidation potentials (tested up to 30 times) with a 14% loss in activity for H_2 oxidation and a 66% decay in the H_2 production current (Figure S19). As shown in Figure 7, the onset potentials corresponding to H_2 oxidation and production are non-overlapping and the half-peak potentials are separated by nearly 1 V, indicating that both reactions can be sustained with a single starting complex, although catalysis may involve different mechanisms, different conformations, or different species.

SUMMARY

In summary, we have demonstrated that incorporating the amino acid glycine into the P_2N_2 ligand imparts water solubility to this class of molecular electrocatalysts while creating a simple proton channel connecting the second and outer coordination spheres. This proton channel enhances proton transfer from the metal to the solvent via the carboxylic acids and may contribute to both the high activity and low overpotential for H_2 oxidation. The observation of H_2 production from the same starting complex makes this system one of the few catalysts active for both H_2 production and oxidation reported to date.[24] These results demonstrate the value of including an outer coordination sphere with enzyme-like functionality in a molecular electrocatalyst, a finding that likely extends to many types of catalytic systems.

MATERIALS AND METHODS

General Procedures. All samples were prepared under an N_2 atmosphere using either a standard single-manifold Schlenk line or glovebox. Reaction solvents except methanol were dried using an Innovative Technologies Pure Solv solvent purification system. CD_3CN was vacuum transferred from P_2O_5. $[Bu_4N]PF_6$ was prepared from tba $[Bu_4N]I$ and $[NH_4]PF_6$ (Aldrich) and purified by crystallization from acetone.[25] All other chemicals including anhydrous methanol (Sigma Aldrich, sure seal) were used as received. Water was dispensed from a Millipore Milli-Q purifier (ρ = 18 MΩ cm) and sparged with nitrogen. Elemental analyses were performed by Atlantic Microlab, Norcross, GA, with V_2O_5 as a combustion catalyst. Samples for gas chromatography (GC) were collected from the top of a J. Young NMR tube and run on an Agilent Technologies 6850 Network GC system with argon as carrier gas. The system was referenced with a standard gas mixture (CO (5%), H_2 (0.5%), CO_2 (1%), and N_2 (93.5%)). Optical spectroscopy of the samples was recorded using an Ocean Optics USB2000+ miniature fiber-optic spectrometer with a 1 cm quartz cuvette.

NMR Spectroscopy. Solution-state ^1H and ^{31}P NMR spectra were recorded on Varian VNMR spectrometers (300 or 500 MHz ^1H frequency). All ^1H chemical shifts were internally calibrated to the monoprotic solvent impurity, whereas concentrated H_3PO_4 was used as an external reference for ^{31}P NMR shifts.

Mass Spectrometry. MS analysis was performed using a LTQ Orbitrap Velos mass spectrometer (Thermo Scientific, San Jose, CA) outfitted with a custom electrospray ionization (ESI) interface. Electrospray emitters were custom-made using 360 μm o.d. × 20 μm i.d. chemically etched fused silica.[26] The ion-transfer tube temperature and spray voltage were 300 °C and 2.2 kV, respectively. Orbitrap spectra (AGC 1x106) were collected from 600 to 2000 m/z at a resolution of 100k or 300−600 m/z at a resolution of 100k. Samples were directly infused using a 250 μL Hamilton syringe at a flow rate of 1 μL/min. $P^{Cy}_2N^{Gly}_2$ and $[Ni^0(P^{Cy}_2N^{Gly*}_2)_2]^-$ were diluted 100× in methanol, and $[Ni^{II}(P^{Cy}_2N^{Gly}_2)_2]^{2+}$ was diluted 100× in acetonitrile.

Synthesis of $P^{Cy}_2N^{Gly}_2$. Bis(hydroxymethyl)cyclohexylphosphine (400 mg, 2.27 mmol) and glycine (170 mg, 2.27 mmol) were dissolved in 20 mL of absolute ethanol in a Schlenk flask and heated at 70 °C for 15 h. The solvent was removed under reduced pressure and a white solid powder was obtained. The product was collected on a fritted funnel by vacuum filtration and was washed thoroughly with acetonitrile followed by drying under vacuum. Yield: 365 mg (0.84 mmol, 74%). ^1H NMR (D_2O): δ 1.05−1.75 ppm (H-*Cy*; 22H, m); 3.41−3.60 ppm (-PC*H*$_2$N; 8H, b); 4.03 ppm (NC*H*$_2$COOH; 4H, s).^{13}C (for sample with ^{13}C enriched glycine) (CH_3OH): 60 ppm (NCH_2COOH; 4C, td, J_{CH}: 135 Hz, J_{CC}: 47 Hz); 170 ppm (NCH_2COOH; 4C, d, J_{CC}: 47 Hz). $^{31}P\{^1H\}$ NMR (CH_3OH): δ −43.9 ppm, broad (49%) and −36.6 ppm, sharp (51%). Analytical Calculation for $C_{20}H_{36}N_2O_4P_2$: C, 55.81; H 8.37; N 6.51. Found: C, 54.65; H 8.36; N 6.63. ESI MS: m/z $[P^{Cy}_2N^{Gly}_2 + H]^+$: 431.22 (calcd 431.22).

Synthesis of $[Ni^{II}(P^{Cy}_2N^{Gly}_2)_2]^{2+}$. $[Ni(CH_3CN)_6](BF_4)_2$ (55.0 mg, 0.115 mmol) was dissolved in 3 mL of acetonitrile, added dropwise to a suspension of $P^{Cy}_2N^{Gly}_2$ (100 mg, 0.23 mml) in 10 mL of acetonitrile and stirred overnight. The solution turned violet after the addition of the Ni solution. The solvent was removed under reduced pressure and a reddish violet powder was obtained. It was collected on a fritted filter under vacuum after thorough washing with diethyl ether. Yield: 41 mg (0.038 mmol, 33%). ^1H NMR (CD_3CN): δ 1.33−1.92 ppm (H-*Cy*; 22H,m); 3.27−3.67 ppm (-PC*H*$_2$N; 8H, b); 6 ppm (N*H*$^+$CH$_2$COO$^-$, b); 10 ppm (NCH$_2$COO*H*, b). ^{13}C (for sample with ^{13}C enriched glycine) (CH_3CN): 56 ppm (NCH_2COOH; 4C, td, J_{CH}: 139 Hz, J_{CC}: 50 Hz); 168.4 ppm (NCH_2COOH; 4C, d, J_{CC}: 56 Hz). $^{31}P\{^1H\}$ NMR (CH_3CN): δ 8.5 ppm, broad. ESI MS: m/z $\{[Ni(P^{Cy}_2N^{Gly}_2)_2]^{2+}(-BF_4 + O)\}^+$: 944.37 (calcd 944.40).

Synthesis of $[Ni^0(P^{Cy}_2N^{Gly*}_2)_2]^-$. [See SI for full characterization.] $Ni(P^{Cy}_2N^{Gly}_2)_2(BF_4)_2$ (10.0 mg, 8.4 mmol) was dissolved in 10 mL of unbuffered water (pH 7.0) by stirring for 30 min. The pH of the reddish brown solution was 4.5. After a few hours the solution started changing color to pale yellow and after 24 h the change was complete, accompanied by a reduction in solution pH to 3.5. The solvent was evaporated and the complex was stored under N_2. ^1H NMR (D_2O): δ 1.20−1.85 ppm (H-*Cy*; 44H, m); 2.24 ppm (NC*H*$_2$OH, s, 2H); 3.48−3.71 ppm (-PC*H*$_2$N; 16H, b); 3.58 ppm (NC*H*$_2$COOH; 6H, s). ^{13}C (for sample with ^{13}C enriched glycine) (CH_3CN/H_2O 1:1 mixture): 42 ppm (NCH_2OH; 1C, td, J_{CH} = 137 Hz, J_{CC}: 50 Hz); 56 ppm (NCH_2COOH; 3C, td, J_{CH} = 142 Hz, J_{CC} = 54 Hz); 168.5 (NCH_2COOH, 2C, d, J_{CC} = 52 Hz), 170.6 (HCO_3^-, 1C, d, J_{CH} = 40 Hz), 171.3 ppm (NCH_2COOH, 1C, d, J_{CC} = 52 Hz). $^{31}P\{^1H\}$

NMR: 23 ppm (H_2O). ESI MS (MeOH): m/z $\{[Ni^0(P^{Cy}_2N^{Gly*}_2)_2]^{2+} - 2COOH\}^+$: 818.32 (calcd: 818.42).

Infrared Spectroscopy with Addition of Base. Solution FTIR spectra were recorded using a Nicolet iS10 spectrophotometer (Thermo Scientific) using a liquid cell with CaF_2 windows (path length ~0.1 mm). A 10 mM stock solution of $[Ni^{II}(P^{Cy}_2N^{Gly}_2)]^{2+}$ in methanol was prepared for each data set. Two hundred μL aliquots were first purged with H_2, followed by the addition of 0, 2, 4, 6 or 8 equivalents of tetramethylguanidine (TMG) base. The samples were prepared in the glovebox and ~5 min elapsed between sample preparation and measurement. A similar procedure was followed with an analogous sample of $[Ni^{II}(P^{Cy}_2N^{Gly}_2)_2]^{2+}$ under N_2 atmosphere without adding H_2 (Figure S6B).

NMR Spectroscopy with Addition of Base Titration. ^{31}P NMR spectra were recorded on a 10 mM stock solution of $[Ni^{II}(P^{Cy}_2N^{Gly}_2)_2]^{2+}$ prepared in methanol. First, 600 μL of freshly prepared solution was titrated incrementally with 1.5 and then 8 equiv of triethylamine. The samples were prepared under N_2 atmosphere in a glovebox and the spectrum collected for approximately 2 h before the next base addition (Figure S6A).

Determination of the Diffusion Coefficient. Diffusion measurements were performed at 25 °C on a 300 MHz Agilent VNMRS spectrometer. The system is equipped with a single axis gradient probe that has a maximum gradient strength of 20 G/cm. Gradient calibration utilized a standard sample (1% H_2O in 99% D_2O) that yielded a diffusion coefficient of 1.9×10^{-5} cm^2/s for H_2O using the bipolar pulsed-field-gradient sequence. The NMR signal attenuates as described by the Stejskal–Tanner equation:[27]

$$I = I_0 e^{-D\gamma^2 g^2 \delta^2 (\Delta - \frac{\delta}{3})} \quad (3)$$

where I_0 denotes the signal intensity in the absence of gradient, γ is the gyromagnetic ratio of the studied nuclei, g is the gradient strength, δ is the gradient pulse duration (4 ms), and Δ is the time interval (100–400 ms) between two gradient pairs. In our measurements, we varied the gradient strength from 0 to 20 G/cm in 10 steps with 16 scans at each step. Normal signal attenuation yielded a single diffusion coefficient for the catalyst, with an experimental error bar of <10%. Diffusion experiments used ^1H NMR and were taken on 0.2 mM catalyst solutions in 0.1 M electrolyte at pH 3.5 (unbuffered) and pH 7 (buffered).

Titration Experiments. A solid-state pH meter (IQ150 hand-held pH/mV/temperature meter, IQ instruments) was used for all the pH measurements during the experiment with constant stirring of the solution. First, a 10 mL aqueous solution of 0.5 mM of $[Ni^0(P^{Cy}_2N^{Gly*}_2)_2]^-$ (containing 0.1 M $NaClO_4$) was prepared under N_2 atmosphere. The pH of the solution was 3.6. The pH was adjusted to 1.8 with the addition of ~5 μL of 11.6 M $HClO_4$. The solution was then titrated with NaOH (0.1 M) while monitoring the pH, until the pH stabilized at 10.0. A similar experiment was then repeated under H_2 (1 atm). Titration data is shown in Figure S12 with inflection points corresponding to deprotonation of the four COOH groups (average pK_a = 2.5) and two NH groups (average pK_a = 6.8) groups indicated. In an analogous experiment, $[^{NiII}(P^{Cy}_2N^{Gly}_2)_2]^{2+}$ was dissolved in methanol (0.5 mM) and excess HDMF triflate was added to adjust the pH to ~0. The solution was titrated with triethylamine. A broad change over the pH region was observed, signifying close pK_a values for the pendant amine (~6) and carboxylic acid (~4) groups compared to water (Figure S11).

Electrochemistry. Cyclic voltammetry and chronoamperometry experiements were performed on a CH Instruments 1100A or 600D electrochemical analyzer using a standard three-electrode cell configuration. The working electrode was a polyether–ether ketone-encased glassy carbon disk (1 mm diameter, ALS) polished using diamond paste (0.25 μm, Buehler). The reference electrode was a AgCl-coated Ag wire suspended in electrolyte solution and separated from the analyte compartment by a Vycor frit. The counterelectrode was a glassy carbon rod (3 mm, Alfa Aesar). All couples were referenced to the ferrocenium/ferrocene couple ($FeCP_2^{+/0}$) at 0.0 V, with ferrocene added as internal standard in acetonitrile or methanol and with hydroxymethylferrocene added ($E_{1/2,Fe(III/II)}$ = −0.073 V vs $FeCP_2^{+/0}$) as the standard for aqueous measurements.[28]

Voltammetry was recorded on solutions of $[Ni^{II}(P^{Cy}_2N^{Gly}_2)_2](BF_4)_2$ (0.2 mM unless otherwise specified) in water (0.1 M $Na[ClO_4]$), methanol (0.1 M $[Bu_4N]PF_6$) or acetonitrile (0.1 M $[Bu_4N]PF_6$) The buffer solutions with pH at 3.5, 5, 6, 7, and 9, were prepared using 0.1 M of 2-morpholinoethanesulfonic acid (MES) and (4-(2-hydroxyethyl)-1-piperazineethanesulfonic acid (HEPES) mixture (1:1) buffer followed by adjusting the pH using dilute NaOH and dilute acetic acid aqueous solutions.

Voltammograms with scan rates from 0.05 to 5 V/s were taken at each pH, under both N_2 and H_2. Under H_2, catalytic current enhancements were observed without added base so only a single catalytic voltammogram was collected for each pH value.

Determination of the Surface Area of the Electrode. Chronoamperometric measurements of the oxidation of ferrocenium were performed on four independently prepared solutions of ferrocene (0.98–1.45 mM) in acetonitrile (0.1 M $[Bu_4N]PF_6$). Background-subtracted traces were fitted using the Cottrell equation (eq S2, Figure S15) to obtain the area of the working electrode, taking $D = 2.4 \times 10^{-5}$ cm^2/s as the diffusion coefficient for ferrocene in acetonitrile.[29]

■ ASSOCIATED CONTENT

Supporting Information

General procedures; synthesis and characterization of Ni-$(P^{Cy}_2N^{Gly*}_2)_2^0$ [^{13}C and $^{31}P\{^1H\}$ NMR spectra, XPS (for Ni 2p region) spectra, optical spectra]; electrochemistry controls; FTIR spectra of $P^{Cy}_2N^{Gly}_2$ and $[Ni(P^{Cy}_2N^{Gly}_2)_2]^{2+}$ in MeOH; titration data in methanol and water. This material is available free of charge via the Internet at http://pubs.acs.org.

■ AUTHOR INFORMATION

Corresponding Authors

john.roberts@pnnl.gov
wendy.shaw@pnnl.gov

Notes

The authors declare no competing financial interest.

■ ACKNOWLEDGMENTS

This work was funded by the Office of Science Early Career Research Program through the U.S. Department of Energy (DOE), Basic Energy Sciences (BES) (A.D., S.L., W.J.S.), and the Center for Molecular Electrocatalysis, an Energy Frontier Research Center funded by the U.S. DOE, BES (J.H., J.A.S.R.). Part of the research was conducted at the W.R. Wiley Environmental Molecular Sciences Laboratory, a national scientific user facility sponsored by U.S. DOE's Office of Biological and Environmental Research program located at Pacific Northwest National Laboratory (PNNL). PNNL is operated by Battelle for the U.S. DOE.

■ REFERENCES

(1) (a) Fontecilla-Camps, J. C.; Volbeda, A.; Cavazza, C.; Nicolet, Y. *Chem. Rev.* **2007**, *107*, 4273–4303. (b) Madden, C.; Vaughn, M. D.; Diez-Perez, I.; Brown, K. A.; King, P. W.; Gust, D.; Moore, A. L.; Moore, T. A. *J. Am. Chem. Soc.* **2012**, *134*, 1577–1582. (c) Vincent, K. A.; Parkin, A.; Armstrong, F. A. *Chem. Rev.* **2007**, *107*, 4366–4413.

(2) (a) Goldet, G.; Wait, A. F.; Cracknell, J. A.; Vincent, K. A.; Ludwig, M.; Lenz, O.; Friedrich, B.; Armstrong, F. A. *J. Am. Chem. Soc.* **2008**, *130*, 11106–11113. (b) Leger, C.; Jones, A. K.; Roseboom, W.; Albracht, S. P. J.; Armstrong, F. A. *Biochemistry* **2002**, *41*, 15736–15746. (c) Parkin, A.; Goldet, G.; Cavazza, C.; Fontecilla-Camps, J. C.; Armstrong, F. A. *J. Am. Chem. Soc.* **2008**, *130*, 13410–13416.

(3) Rakowski DuBois, M.; DuBois, D. L. *Chem. Soc. Rev.* **2009**, *38*, 62–72.

(4) (a) Gunner, M. R.; Mao, J.; Song, Y.; Kim, J. *Biochim. Biophys. Acta* **2006**, *1757*, 942−968. (b) Karlin, S.; Zhu, Z. Y.; Karlin, K. D. *Proc. Natl. Acad. Sci. U.S.A.* **1997**, *94*, 14225−14230. (c) Maglio, O.; Nastri, F.; Martin de Rosales, R. T.; Faiella, M.; Pavone, V.; DeGrado, W. F.; Lombardi, A. *C. R. Chim.* **2007**, *10*, 703−720. (d) Miner, K. D.; Mukherjee, A.; Gao, Y. G.; Null, E. L.; Petrik, I. D.; Zhao, X.; Yeung, N.; Robinson, H.; Lu, Y. *Angew. Chem.* **2012**, *51*, 5589−5592. (e) Motherwell, W. B.; Bingham, M. J.; Six, Y. *Tetrahedron* **2001**, *57*, 4663−4686. (f) Ward, T. R. *Acc. Chem. Res.* **2011**, *44*, 47−57.

(5) (a) Gloaguen, F.; Rauchfuss, T. B. *Chem. Soc. Rev.* **2009**, *38*, 100−108. (b) Shaw, W. J.; Helm, M. L.; DuBios, D. L. *Biochim. Biophys. Acta: Bioenergetics* **2013**, *1827*, 1123−1139.

(6) Peters, J. W.; Lanzilotta, W. N.; Lemon, B. J.; Seefeldt, L. C. *Science* **1998**, *282*, 1853−1858.

(7) (a) Jain, A.; Lense, S.; Linehan, J. C.; Raugei, S.; Cho, H.; Dubois, D. L.; Shaw, W. J. *Inorg. Chem.* **2011**, *50*, 4073−4085. (b) Jain, A.; Reback, M. L.; Lindstrom, M. L.; Thogerson, C. E.; Helm, M. L.; Appel, A. M.; Shaw, W. J. *Inorg. Chem.* **2012**, *51*, 6592−6602. (c) Reback, M. L.; Ginovska-Pangovska, B.; Ho, M.-H.; Jain, A.; Squier, T. C.; Raugie, S.; Roberts, J. A. S.; Shaw, W. J. *Chem.—Eur. J.* **2013**, *19*, 1928−1941.

(8) (a) Lense, S.; Ho, M.-H.; Chen, S.; Jain, A.; Raugei, S.; Linehan, J. C.; Roberts, J. A. S.; Appel, A. M.; Shaw, W. J. *Organometallics* **2012**, *31*, 6719−6731. (b) Wilson, A. D.; Newell, R. H.; McNevin, M. J.; Muckerman, J. T.; Rakowski DuBois, M.; DuBois, D. L. *J. Am. Chem. Soc.* **2006**, *128*, 358−366. (c) Yang, J. Y.; Chen, S.; Dougherty, W. G.; Kassel, W. S.; Bullock, R. M.; DuBois, D. L.; Raugei, S.; Rousseau, R.; Dupuis, M.; Rakowski DuBois, M. *Chem. Commun.* **2010**, *46*, 8618−8620.

(9) Li, X.; Pecoraro, V. L. *Inorg. Chem.* **1989**, *28*, 3403−3410.

(10) Bard, A. J.; Faulkner, L. R. *Electrochemical Methods. Fundamentals and Applications.*; John Wiley & Sons, Inc.: Hoboken, NJ, 2001.

(11) (a) Yang, J. Y.; Bullock, R. M.; Shaw, W. J.; Twamley, B.; Fraze, K.; Rakowski DuBois, M.; DuBois, D. L. *J. Am. Chem. Soc.* **2009**, *131*, 5935−5945. (b) O'Hagan, M.; Ho, M.-H.; Yang, J. Y.; Appel, A. M.; DuBois, M. R.; Raugei, S.; Shaw, W. J.; DuBois, D. L.; Bullock, R. M. *J. Am. Chem. Soc.* **2012**, *134*, 19409−19424.

(12) Seu, C. S.; Appel, A. M.; Doud, M. D.; DuBois, D. L.; Kubiak, C. P. *Energy Environ. Sci.* **2012**, *5*, 6480−6490.

(13) Binding a fifth ligand should place Ni into a trigonal bipyramidal coordination geometry, resulting in inequivalent P atoms, as observed in X-ray structures of other $[Ni^{II}(P_2N_2)_2]^{2+}$ having cyclohexyl groups on P.[8] A single sharp ^{31}P resonance with $[Ni^{II}(P^{Cy2}N^{Gly2})_2]^{2+}$ is observed in methanol with 1.5−8 equiv of base added (Figure S6), indicating the equivalence of all phosphorous atoms and the lack of a strongly bound COO^-.[7a,b] FTIR data show a small new band upon the addition of 8 equiv of base which could be due to a transient interaction of COO^- with Ni^{2+} (Figure S6).

(14) (a) Nakamoto, K. *Infrared and raman spectra of inorganic and coordination compounds*, 4th ed.; Wiley-Interscience: New York, 1986. (b) Silverstein, R. M.; Webster, F. X.; Kiemle, D. J. *Spectrometric identification of organic compounds*; John Wiley and Sons, Inc.: New York, 2005. (c) Max, J.-J.; Chapados, C. *J. Phys. Chem. A* **2004**, *108*, 3324−3337. (d) Gomez-Zavaglia, A.; Fausto, R. *Phys. Chem. Chem. Phys.* **2003**, *5*, 3154−3161.

(15) O'Hagan, M.; Shaw, W. J.; Raugei, S.; Chen, S.; Yang, J. Y.; Kilgore, U. J.; DuBois, D. L.; Bullock, R. M. *J. Am. Chem. Soc.* **2011**, *133*, 14301−14312.

(16) It should be noted that direct comparisons between the pK_a values determined in different solvents are not necessarily relevant, and in this case are only used to compare them to other pK_a values in the same solvent.

(17) O'Hagan, M.; Ho, M.-H.; Yang, J. Y.; Appel, A. M.; Rakowski DuBois, M.; Raugei, S.; Shaw, W. J.; DuBois, D. L.; Bullock, R. M. *J. Am. Chem. Soc.* **2012**, *134*, 19409−19424.

(18) DuBois, D. L.; Bullock, R. M. *Eur. J. Inorg. Chem.* **2011**, 1017−1027.

(19) Artero, V.; Fontecave, M. *Chem. Soc. Rev* **2013**, *42*, 2338−2356.

(20) Pool, D. H.; Stewart, M. P.; O'Hagan, M.; Shaw, W. J.; Roberts, J. A. S.; Bullock, R. M.; DuBois, D. L. *Proc. Natl. Acad. Sci. U.S.A.* **2012**, *109*, 15634−15639.

(21) Yang, J. Y.; Smith, S. E.; Liu, T.; Dougherty, W. G.; Hoffert, W. A.; Kassel, W. S.; Bullock, R. M.; Rakowski DuBois, M.; DuBois, D. L. *J. Am. Chem. Soc.* **2013**, *135*, 9700−9712.

(22) Raugei, S.; Chen, S.; Ho, M.-H.; Ginovska-Pangovska, B.; Rousseau, R. J.; Dupuis, M.; DuBois, D. L.; Bullock, R. M. *Chem.—Eur. J.* **2012**, *18*, 6493−6506.

(23) Joo, F. *Aqueous Organometallic Catalysis*; Kluwer Academic Publishers: Dordrecht, 2001; Vol. *23*.

(24) (a) Smith, S. E.; Yang, J. Y.; DuBois, D. L.; Bullock, R. M. *Angew. Chem.* **2012**, *51*, 3152−3155. (b) Tran, P. D.; Goff, A. L.; Heidkamp, J.; Jousselme, B.; Guillet, N.; Palacin, S.; Dau, H.; Fontecave, M.; Artero, V. *Angew. Chem.* **2011**, *50*, 1371−1374.

(25) Fry, A. J. In *Laboratory Techniques in Electroanalytical Chemistry*, 2nd ed.; Kissinger, P. T., Heineman, W. R., Eds.; Marcel Dekker, Inc.: New York, 1996; pp 469−483.

(26) Kelly, R.; Page, J.; Luo, Q.; Moore, R.; Orton, D.; Tang, K.; Smith, R. *Anal. Chem.* **2006**, *78*, 7796−7801.

(27) Stejskal, E. O.; Tanner, J. E. *J. Chem. Phys.* **1965**, *42*, 288−292.

(28) Hoffert, W. A.; Roberts, J. A. S.; Bullock, R. M.; Helm, M. L. *Chem. Commun.* **2013**, in press.

(29) Kadish, K. M.; Ding, J. Q.; Malinski, T. *Anal. Chem.* **1984**, *56*, 1741−1744.